Fowler-Nordheim-like local injection of photoelectrons from a silicon tip

A. C. H. Rowe and D. Paget[*]

Laboratoire de Physique de la Matière Condensée, École Polytechnique, 91128 Palaiseau Cedex, France
(Received 7 December 2006; published 12 March 2007)

Tunneling between a photoexcited *p*-type silicon tip and a gold surface is studied as a function of tip bias, tip-sample distance, and light intensity. In order to extend the range of application of future spin injection experiments, the measurements are carried out under nitrogen gas at room temperature. It is found that, while tunneling of valence band electrons is described by a standard process between the semiconductor valence band and the metal, the tunneling of photoelectrons obeys a Fowler-Nordheim-like process directly from the conduction band. In the latter case, the bias dependence of the photocurrent as a function of distance is in agreement with theoretical predictions which include image charge effects. Quantitative analysis of the bias dependence of the dark and photocurrent spectra gives reasonable values for the distance, and for the tip and metal work functions. For small distances image charge effects induce a vanishing of the barrier, and the bias dependence of the photocurrent is exponential. In common with many works on field emission, fluctuations in the tunneling currents are observed. These are mainly attributed to changes in the prefactor for the tunneling photocurrent, which we suggest is caused by an electric-field-induced modification of the thickness of the natural oxide layer covering the tip apex.

I. INTRODUCTION

Although the photosensitivity of tunnel processes between a metal and a semiconductor has been widely considered,[1–3] the majority of these investigations concern the effect of surface photovoltage on tunneling between a metallic tip and a planar semiconducting surface. On the other hand, the mechanisms governing injection of photoelectrons from a semiconducting tip under light excitation into a planar metallic surface are less well studied despite the fact that a proper understanding is important both from a fundamental viewpoint, and for a variety of potential applications.

Photoexcited semiconducting tips can in principle be used as local spin injectors since circularly polarized light produces a spin-polarized electron population via optical pumping.[4] The mean spin of the tunnel-injected electrons can then be controlled via a change in the light helicity. There exist numerous potential applications for a spin injector of this type, such as spin-polarized scanning tunneling microscopy (SPSTM),[5] quantum computing,[6] and spintronics,[7] none of which has been convincingly demonstrated. While it is known that a change in pump light helicity modifies the tunnel junction resistance between a ferromagnetic metallic tip and a photoexcited GaAs surface via the spin dependence of the tunneling process,[8] spurious optical effects in photoexcited semiconductor tips have been blamed for the apparent observation of nonzero spin polarizations, even on nonmagnetic surfaces.[9,10] In order to better understand *nonpolarized* photoassisted tunneling from a semiconductor tip into a metallic surface a number of groups[11] commenced by studies of the tip bias, distance, and light intensity dependence of the injected current. Perhaps the most detailed investigations, both theoretical and experimental, were performed by Prins *et al.*[12] For relatively small tip bias up to about 0.5 V, tunneling current spectra were interpreted using a model that considered both the characteristics of the space charge layer formed at the tip surface, and of the tunnel

barrier itself. While this model can account for a number of observed phenomena, its extension to include spin-polarization effects has met with less success.[9,13]

A second related area of interest is the emission of electrons from high-aspect-ratio objects such as semiconducting[14–16] or carbon nanotube tips,[17] as well as the influence of photoexcitation on the emitted current.[18] While the electric fields are similar to those used in tunneling experiments, the tip-sample (or rather the cathode-anode) distances are typically much larger (up to several micrometers). Under these conditions, the emitted current is usually described by a Fowler-Nordheim (FN) process[19] from surface states to vacuum states. Unless a complex sample (anode) structure is used,[20] this process is spin independent since the vacuum states are themselves unpolarized. The bias dependence of the FN current is of the form[19,21]

$$I = A(V)/(\gamma V)^2 \times \exp[-B(V)/\gamma V], \tag{1}$$

where $A(V)$ and $B(V)$ are slowly varying functions of bias. The quantity γ, larger than unity for sharp tips, describes the geometrical enhancement of the electric field.[21]

In the present paper we investigate the mechanisms that govern photoelectron injection from a semiconducting tip. The tip bias value, as large as −3 V, is sufficient to induce an increase in the injected current by FN tunneling, but not large enough to enable observation of current oscillations related to quantized states in the tunneling gap.[22] Here, we are not interested in spin-polarized injection so silicon tips and gold surfaces are used. With respect to a number of previous works on tunnel injection of photocarriers,[9,10,12,13,23] the present situation is simpler for four reasons: (i) The light excitation is incident on the rear planar surface of the tip, which itself is situated at the end of a very stiff cantilever (see Fig. 1). Consequently, the photoelectrons diffuse from the rear of the tip (where they are created) to the tip apex, and the number of photoelectrons reaching the tip apex is independent of tip bias. This is at variance with studies
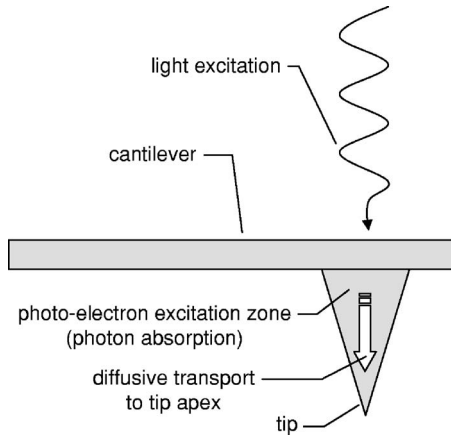
FIG. 1. Injection geometry: A semiconducting tip, placed at the end of an AFM-like cantilever, is excited by light impinging on its rear planar face.

FIG. 2. (a) Schema of the band structure of the semiconductor (left) and of the metal (right) for a tip bias V. Arrow 1 represents the dark current arising from a tunneling process between the semiconductor valence band and the metal. Arrow 3 represents the current arising from a tunneling process between localized midgap semiconductor states and the metal, as proposed in Ref. 12. Arrow 2 shows the observed FN-like tunneling process of photoelectrons from the semiconductor conduction band. (b) Tunnel barrier shape with (solid line) and without (dotted line) image charge effects.

where the light excitation is incident on the front face of the tip apex,[12,13] and the injected photocurrent depends on tip bias via the bias-dependent depletion layer width.[24] The experiment reported here thus resembles an atomic force microscope (AFM), with the exception that tip-sample distance is controlled using the tunnel current.[25] (ii) The use of p^+-doped tips guarantees that the conductivity of the tip is high and that most of the applied bias is dropped across the tunnel barrier itself. The experimental results can then be understood using a relatively simple theory. (iii) The tip-surface barrier (V_b) can be neglected for $V > V_b$. (iv) The experiments are performed in an inert gas atmosphere. Although this has intrinsic drawbacks compared with ultrahigh-vacuum conditions, in particular related to possible tip pollution and current instabilities caused by changes in the native oxide layer thickness, the choice is deliberately made in order to simplify and extend the scope of application of future SPSTM studies.[26]

The dependence of the tunneling dark current and photocurrent as a function of bias, tip-sample distance, and excitation light intensity is investigated. It is found that (i) the dark current obeys a standard tunneling process between the valence band of the semiconductor and the metallic local density of states, and (ii) the tunneling photocurrent occurs directly from the conduction band of the semiconductor to the metallic states through a FN-like process and not, as found by Prins et al. for GaAs tips,[12] via a standard tunneling process from midgap states at the semiconductor surface. The implications of these findings for spin-polarized tunneling are discussed.

II. THEORETICAL CONSIDERATIONS

The following section describes tunnel injection between a negatively biased, p^+-doped photoexcited semiconducting tip and a metallic surface. Shown in Fig. 2(a) is a schema of the band structure of the tip and metallic surface at applied tip bias V. Light excitation from the rear of the tip results in the formation of a steady state population of photoelectrons in the conduction band. Since the tip is highly conductive,
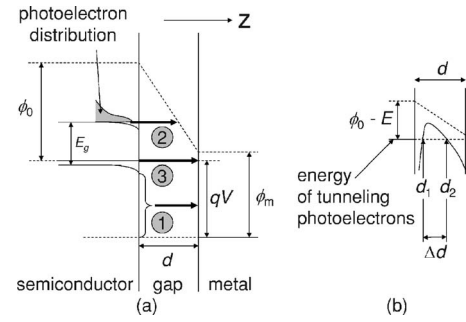
the semiconductor band structure is independent of bias and is simply shifted with respect to the metallic one by qV, where $q < 0$ is the electronic charge.

Shown in Fig. 2(b) is a schematic of the shape of the tunneling barrier. Because of image charge effects,[27] the tunneling barrier at the energy of the tunneling electrons extends between d_1 and d_2, and its width $\Delta d = d_2 - d_1$ is smaller than the physical tip-sample distance d.

Because the applied tip bias is negative, the dark current and the current of minority photocarriers are described by a tunneling of electrons from the semiconductor to the metal. The incremental tunnel current from an occupied energy level E in the tip to an empty level in the metal at the same energy is given by[27,28]

$$\delta I_t = KS\rho_s\rho_m \exp(-\kappa\Delta d), \qquad (2)$$

where ρ_s and ρ_m are the densities of states at E of the semiconductor and of the metal respectively, and S is the tip surface area. The quantity K is proportional to the tunneling matrix element, and depends on the electronic orbitals of tip and surface via which tunneling occurs. The inverse distance for the exponential decay of the tunneling current is given by[27]

$$\kappa = 2\frac{\sqrt{2m}}{\hbar}\sqrt{\bar{\phi} - E}, \qquad (3)$$

where m is the mass of the electron in vacuum. Here, the zero of energy is taken at the Fermi level of the semiconductor. In the work of Simmons,[27] E is the sum of the potential energy of the tunneling electrons and their kinetic energy oriented perpendicular to the surface E_z. In the present case, since tunneling from a tip is essentially a unidirectional process,[29] the tunneling electrons have a velocity along the tip axis and $E_z = E$. Equation (3) expresses the highly simplifying result that tunneling across a barrier of complex spatial shape mostly depends on the spatial average of the barrier, defined as

$$\bar{\phi} = \frac{1}{\Delta d} \int_{d_1}^{d_2} \phi(z) dz. \qquad (4)$$

A. Tunneling photocurrent

In general the tunneling current obtained from Eqs. (2), (3), and (4) is given by the expression

$$I_{ph} = A_{ph} \exp(-\kappa_{ph} d). \qquad (5)$$

The prefactor A_{ph} is found by replacing ρ_s by the concentration N_e of photoelectrons (a quantity proportional to the excitation light power):

$$A_{ph} = K_{ph} S N_e \rho_m. \qquad (6)$$

For a standard tunneling current in the absence of image charge effects one has $\bar{\phi} = \phi_0 - qV^*/2$. Since the photoexcitation is only slightly above gap, E is the semiconductor band gap energy E_g and κ_{ph} is given by

$$\kappa_{ph} = 2\sqrt{\frac{2m}{\hbar}}(\chi_0 - qV^*/2), \qquad (7)$$

where $\chi_0 = \phi_0 - E_g$ is the affinity of the tip surface. The effective tip bias V^* is given by

$$V^* = V + V_0 = V + \frac{1}{q}(\phi_0 - \phi_m) \qquad (8)$$

since there is an electric field at $V=0$ between tip and surface if ϕ_m is different from ϕ_0 ($\phi_0 - \phi_m \approx -0.6$ eV for clean surfaces of silicon and gold).

At larger tip bias, tunneling from the semiconductor to the metal can occur via vacuum states [see Fig. 2(a), arrow 2]. This process resembles FN emission with three differences with respect to Eq. (1) and will therefore be denominated FN-like. First, in cases where the tip-sample distance is small compared with the radius of curvature of the tip, no field enhancement occurs at the semiconducting tip [i.e., $\gamma = 1$ in Eq. (1) as explained in the Appendix]. A second difference from the field emission process is the replacement of V by V^* given by Eq. (8) [in field emission studies $\phi_0 - \phi_m$ is negligible compared to the applied tip (cathode) bias and can be ignored]. Finally, since the tunneling photoelectrons are distributed over a narrow energy range at the bottom of the conduction band, it is not necessary to perform an integration over energy. Unlike the case of Eq. (1), the prefactor is independent of tip bias so that Eq. (5) is still valid, albeit with a modified value of κ_{ph}.

1. FN-like tunneling without image charge effects

In order to observe FN-like tunneling, qV^* must be larger than $\phi_0 - E_g$, so that the threshold bias V_{th} is

$$qV_{th} = \phi_m - E_g. \qquad (9)$$

The spatial average $\bar{\phi}$ of the barrier potential[30] is then equal to $(\phi_0 + E_g)/2$. The tunneling photocurrent is obtained from a calculation of the quantum tunneling probability at E_g, and is given by Eq. (5) with

$$\kappa_{ph} = 2\frac{\sqrt{m}}{\hbar}\frac{\chi_0^{3/2}}{qV^*}. \qquad (10)$$

If V_0 is negligible with respect to V, Eq. (10) indicates that a plot of I_{ph} in logarithmic units as a function of $1/V$ should be linear. The slope of this line should decrease when d is decreased. For a bias lower than V_{th}, the photocurrent has a smaller value obtained from Eqs. (5) and (7).

2. FN-like tunneling with image charge effects

Inclusion of image charge effects requires a modification of Eq. (10). It is not a bad approximation to apply the treatment of Simmons for tunneling between two metals,[27] since with respect to the static dielectric constant of vacuum ($\epsilon = 1$), that of silicon ($\epsilon = 13$) can be approximated by that of a metal ($\epsilon \rightarrow \infty$). The image charge potential is given by[27]

$$\phi(z) = \phi_0 - \frac{qV^*z}{d} - 1.15\frac{\lambda d^2}{z(d-z)}, \qquad (11)$$

where λ describes the magnitude of the image charge effects:

$$\lambda = \frac{q^2 \ln(2)}{8\pi\epsilon\epsilon_0 d}. \qquad (12)$$

Here ϵ_0 is the permittivity of free space. For qV^* sufficiently large[31] and $d_1 \ll d$, one finds that the inverse distance for tunneling is now given by

$$\kappa_{ph} = 2\frac{\sqrt{m}}{\hbar}\frac{\chi_0^{3/2}(1 - 5.6\lambda/\chi_0)}{qV^*}\sqrt{1 + 5.6\lambda/\chi_0 - aqV^*/\chi_0}, \qquad (13)$$

where

$$a = \frac{\lambda}{\chi_0}\left[1.2 - \frac{2.3}{1 - 5.6\lambda/\chi_0}\ln\left(\frac{d_2 d}{d_1(d - d_2)}\right)\right] \qquad (14)$$

is weakly dependent on V^* via the logarithmic term. An approximate[31] but physically meaningful expression for the threshold bias V_{th} for FN-like tunneling is found by setting $d_2 = d$ which gives

$$qV_{th} = \phi_m - E_g - 5.6\lambda, \qquad (15)$$

which decreases with decreasing d, unlike the value given by Eq. (9). As expected, if $\lambda \ll \chi_0$, Eq. (13) reduces to Eq. (10) and Eq. (15) reduces to Eq. (9).

The inclusion of image charge effects modifies the photocurrent in two ways. (i) At small bias, because of the dependence of κ_{ph} on d in Eq. (13), the slope of $\log(I_{ph})$ as a function of $1/V$ is no longer proportional to d unless this distance is large. The effective tip affinity χ_0^* is now given by $\chi_0^{*3} = (\chi_0 + 5.6\lambda)(\chi_0 - 5.6\lambda)^2$. (ii) If $aqV^* \approx \chi_0 + 5.6\lambda$ the lowering of the barrier due to image charges causes an excess photocurrent.

B. Tunneling dark current

As represented in Fig. 2, the dark current is presumed to occur from tunneling processes between occupied states in
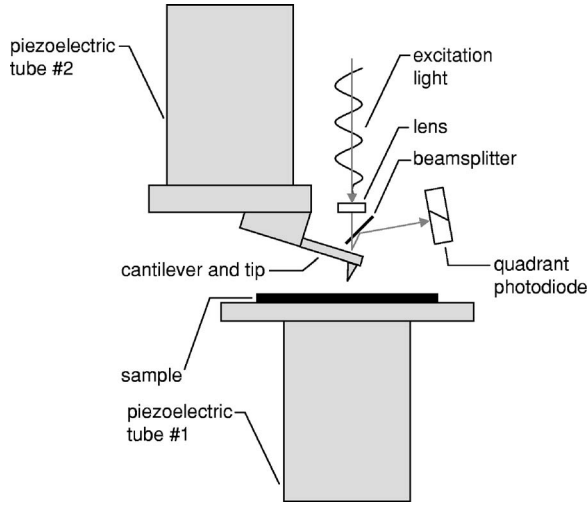
FIG. 3. Schema of the atomic-force-microscope-like experimental setup. The sample is fixed on a piezoelectric tube, enabling scans in the plane of the sample. The cantilever holding the tip is fixed on a second piezoelectric tube enabling motions in the vertical direction.

the semiconductor valence band and empty states in the metal at the same energy. At valence band energies, image charge effects[32] and FN-like tunneling can be neglected. An energy-independent density of states for the metal is assumed,[33] and the usual form of ρ_s for a bulk semiconductor is used, $\rho_s(E) = (1/2\pi^2)(2m^*/\hbar^2)^{3/2}\sqrt{-E}$, where $\hbar$ is Planck's constant, m^* is the effective electronic mass, and $E < 0$ is the energy of the tunneling electrons in the valence band. The value of the dark current is obtained by integrating Eq. (2) between the Fermi level of the semiconductor and that of the metal,

$$I_{dark} = A_{dark} \int_{-qV}^{0} \sqrt{-E}\, \exp(-\kappa_{dark}d)dE \qquad (16)$$

where κ_{dark} and A_{dark} are given, respectively, by

$$\kappa_{dark} = 2\sqrt{\frac{2m}{\hbar}(\phi_0 - E - qV^*/2)} \qquad (17)$$

and

$$A_{dark} = K_{dark}\frac{S\rho_m}{2\pi^2}\left(\frac{2m^*}{\hbar^2}\right)^{3/2}. \qquad (18)$$

The dark current is the sum of several exponential contributions and generally does not have a simple exponential dependence as a function of distance.

III. EXPERIMENTAL DETAILS

Experiments were conducted in a tailor-made system enabling STM as well as AFM investigations at room temperature, and consistent with the geometry of photoelectron injection described in Fig. 1. This system, shown in Fig. 3. operates in an electromagnetically shielded inert gas environment. Worth mentioning are the following particularities, (i)

The excitation laser (wavelength 780 nm, power 10 mW) is focused on the back planar face of the cantilever, yielding a spot of diameter 50 μm opposite the tip position.[34] (ii) A beam splitter situated between the laser and the cantilever sends the light reflected from the cantilever surface onto a quadrant photodiode, thus enabling simultaneous atomic force, dark current and photocurrent measurements. (iii) Two piezoelectric tubes are used. Scans in the plane of the sample for imaging purposes are performed using the four-electrode piezoelectric transducer (PZT) tube on which the sample is mounted, while the tip-sample distance is changed by a second two-electrode PZT tube on which the block holding the cantilever and tip is mounted. This ensures that the light spot is stationary with respect to the location of the tip. (iv) For current measurements the sample is grounded and the bias is applied to the tip. The tip-sample current is monitored using a high-gain–low-noise amplification circuit placed as close as possible to the tip. After installing the sample and cantilever in an air ambient, a metallic grounded hood is placed over the experiment and dry nitrogen is blown for 20 min prior to, and during, the measurements.

Commercially available tapping-mode silicon cantilevers[35] were used in all experiments. The use of relatively stiff cantilevers (of nominal force constant 16 N/m) minimizes the effect of atomic forces on tip-sample distance, and thereby improves the control of this distance using the tunnel current in a feedback loop. Silicon tips were situated at the free end of the cantilever and ranged in height between 5 and 7 μm, and were p-type doped in the range 10^{20} cm^{-3}. The samples consist of polycrystalline gold films, of thickness approximately 60 monolayers, deposited on (111) silicon substrates by electrochemical methods.[36]

Care was taken in order to minimize fluctuations in the tunnel current due to (photo)electrochemical reactions which can induce changes in the tip characteristics. Anodic tip potentials (forward bias for p-type tips) were avoided since they are known to rapidly generate a thick layer of oxide which prevents the observation of tunnel currents. Several tip passivation treatments were tried in order to render the tip surface inert, including removal of the native oxide with hydrofluoric acid. However, the native oxide layer yielded the most inert surface, and the results reported here were all obtained with naturally oxidized tips. As will be seen, the presence of residual water can still induce electrochemical changes in the tip surface which produce instabilities in the tunneling current.

The measurement sequence is shown schematically in Fig. 4. During $T_1 \approx 0.5$ s (i.e., much longer than the time constant of the feedback loop) the pump laser is switched off and no data acquisition takes place. The tip-sample distance is stabilized at $V_{set} = -2$ V by imposing a dark tunneling current $I_{dark} = I_{set}$ using a standard feedback loop. Spectroscopic measurements of the tunneling current as a function of tip bias are then performed in a rapid sequence of two acquisitions over periods T_2 and T_3, each of which lasts 25 ms. Since these scans induce a change in current, the feedback loop is opened for $T_2 + T_3 = 50$ ms, a period significantly shorter than the time constants over which drift in d occurs. During T_2 the laser is switched on, while during T_3 it is switched off. The tunneling dark current spectrum is that
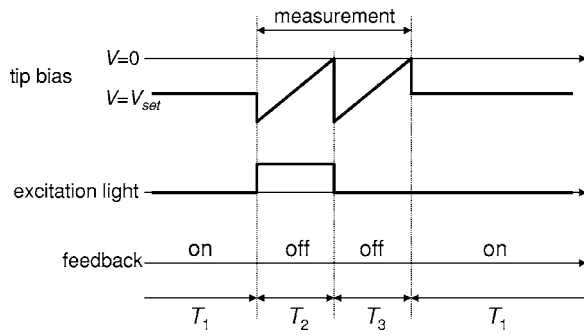
FIG. 4. Measurement sequence (see text).

obtained during T_3, while the tunneling photocurrent spectrum is that obtained by taking the difference of the spectra measured during T_2 and T_3. Most of the results presented in this paper were obtained after only one such acquisition (i.e., without averaging over several spectra).

Using this procedure, the dark current, the photocurrent, and the atomic force between tip and surface (measured using the quadrant photodiode) were simultaneously monitored for increasing tunneling dark currents during T_1, corresponding to decreasing tip-sample distances. In order to check reproducibility and possible current instabilities, each scan was performed ten times in identical conditions.

IV. RESULTS

Figure 5 shows the variation of the atomic force between the tip (shown in the inset of Fig. 6) and the sample, as a function of the tunneling dark current set during time T_1. Shown by arrows in the figure are the selected dark current values for which tunneling spectra will be presented below. The atomic force stays approximately equal to zero up to a dark current of the order of 2 nA, above which it abruptly becomes repulsive because of mechanical contact with the surface. This abruptness as well as the fact that a tunneling current is observed before the onset of a nonzero atomic force are due to the relatively large stiffness of the cantilever.
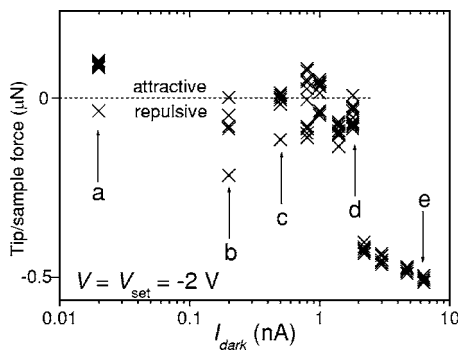

FIG. 5. Dependence of the atomic force between tip and sample as a function of the dark current value imposed during T_1. For each value of I_{dark} ten successive measurements were obtained, each of which is shown in the figure. The arrows $a-e$ correspond to the curves shown in Fig. 8 below. The abrupt change near $I_{dark}=2$ nA is due to mechanical tip-sample contact.
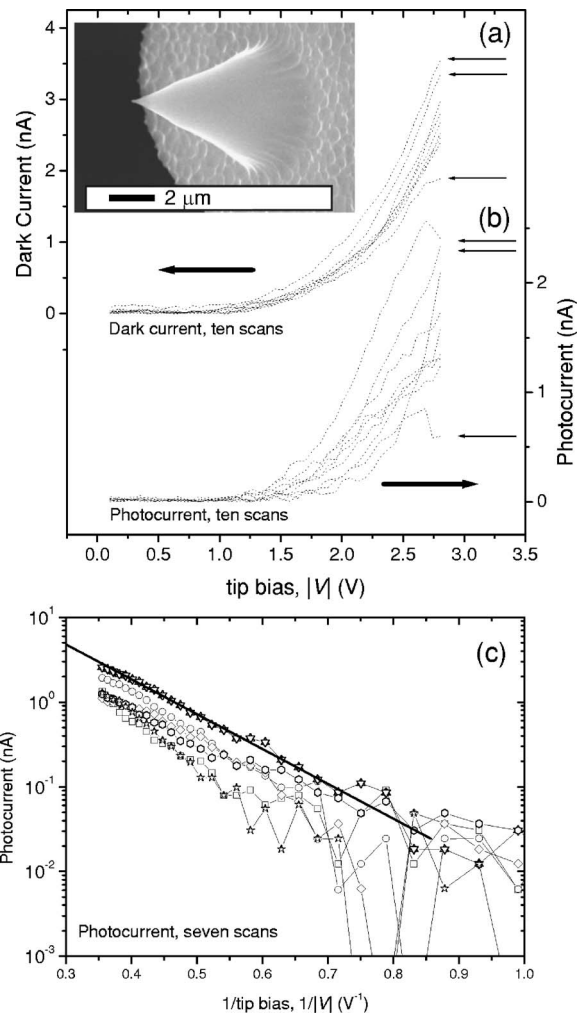

FIG. 6. Ten successive measurements of (a) dark current and (b) photocurrent as functions of tip bias for fixed tip-sample distance. In (a), three curves (designated by arrows) strongly differ from the other curves at V_{set} and were not considered in the analysis. (c) Linear dependence of the photocurrent of the remaining seven curves on a logarithmic plot of the photocurrent versus $1/V$ reveals a FN-like tunnel process. Shown (inset) is a scanning electron microscope image of the sharp tip.

Points a, b, and c correspond to the out-of-contact regime, while point d illustrates the near-contact regime. At point e, there is no doubt that gold indentation occurs since this has been observed[37] for forces as small as several nanonewtons.

A. Instabilities

Shown in Fig. 6(a) are ten dark current spectra at point c in Fig. 5. The corresponding tunneling photocurrent spectra are shown in Fig. 6(b). Both currents strongly increase with bias and no surface photovoltage is observed (no photocurrent is detectable below 1.15 V).

The differences in the curves reveal instabilities in the tunneling process. These instabilities are larger for the tunnel photocurrent, which is consistent with the fact that immediately before the measurement, the feedback imposes a constant dark current I_{dark} at $V=V_{set}$. They manifest themselves
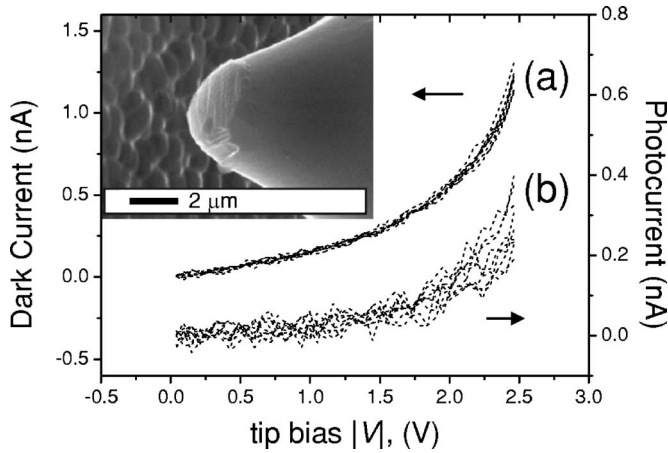
FIG. 7. Blunt tip: Ten successive measurements of (a) dark current and (b) photocurrent as functions of tip bias for fixed, large tip-sample distance. Shown (inset) is a scanning electron microscope image of the tip.

as abrupt temporal changes between a relatively small number of well-defined values which can differ by up to a factor of 3. Such behavior has been reported in works on field emission,[14] on transport in metal-oxide-silicon structures,[38,39] and in tunneling.[40] Since the delay between the instabilities is of the order of a fraction of a second (i.e., much larger than T_2+T_3), no apparent jump is seen within a given curve.

Of the ten dark current spectra in Fig. 6(a), seven curves approximately coincide. The other three curves are discarded since the current value at $V_{set}=-2$ V differs from the setpoint value. As seen from Eqs. (5)–(10), (16), and (18), instabilities can originate from fluctuations in d, (ϕ_0) or (ϕ_m), or the prefactors A_{ph} and A_{dark}. Instabilities in the prefactors can be caused by fluctuations of the tip surface S or of the tunneling probabilities K_{ph} or K_{dark} (it is assumed that N_e and ρ_m are stable).

Instabilities in d can be ruled out based on results obtained with a blunt tip made by mechanically removing the tip apex. The tip is almost ideally flat, with an end diameter of ≈ 2 μm (see inset of Fig. 7). For a blunt tip, tunnel processes are averaged out over a large area and should therefore be relatively insensitive to local changes in geometry and tip-sample surface composition. The spectra shown in Fig. 7 were obtained by fixing the tunneling dark current during T_1 at the same value used for the sharp tip. The dark current spectra are essentially indistinguishable, while differences between photocurrent spectra are comparable to the noise. The same qualitative results are also obtained for all tip-sample distances. This proves that any tip-sample distance noise or drift is effectively compensated by the feedback loop, and therefore that fluctuations in d are not the root cause of current instabilities measured with the sharp tip.

Figure 6(c) shows I_{ph} scans plotted in logarithmic units as a function of $1/V$ for the sharp tip. While I_{ph} varies by up to a factor of 3, the slope [which is related to ϕ_0 according to Eq. (10)] of the curves is the same within experimental error. Variations in ϕ_0 can therefore be ruled out. Fluctuations of A_{dark} can also be excluded using the following reasoning, A change in A_{dark} will induce a change in d via the feedback

loop, and thus a change in the *shape* of $I_{dark}(V)$.[41] This change is not clearly observed [see Fig. 6(a)]. The only remaining possible sources of current fluctuations are changes in A_{ph}, and to some extent in ϕ_m. Since A_{dark} (and thus S) are constant, changes in A_{ph} must originate from changes of the prefactor K_{ph} of Eq. (10).

The same analysis, performed for all distances, shows the following. (i) At large distances (point a of Fig. 5) the instabilities are relatively small. This may be because the local electric field is smaller and thus (photo)electrochemical modification of the surface oxide layer is less important. (ii) For reduced distances before mechanical contact, the instabilities mostly concern K_{ph}. (iii) For measurements performed under mechanical contact (point e of Fig. 5) the instabilities are very large. This is again consistent with the notion that greater electric fields result in an increase in oxide modifying (photo)electrochemical processes. These findings are confirmed by the quantitative analysis presented in Sec. V B, where a possible microscopic interpretation will be proposed.

B. Tunneling processes

The bias dependence of the dark current for different distances is shown in Fig. 8(a), while that of the tunneling photocurrent is shown in Figs. 8(b) and 8(c). For clarity, only curves for which the photocurrent is largest are presented, although the results are typical of a much larger number of experiments. It is apparent that the tunneling dark current and the tunneling photocurrent originate from distinct mechanisms. The tunneling dark current tends to present a flatter spectral response than the photocurrent when plotted against tip bias on a log-linear scale. Furthermore, the slope of the tunneling dark current is relatively insensitive to a change in distance whereas the slope of the tunneling photocurrent spectra increases greatly with an increase in distance.

For curves a, b, and c in Fig. 8(c), the dependence of $\ln(I_{ph})$ as a function of $1/V$ is quasilinear over two orders of magnitude, consistent with Eq. (10) and/or Eq. (13) in the small-bias regime. The tunneling photocurrent behavior is thus consistent with the FN-like process described in Sec. II whereas it will be seen that the tunneling dark current is better described by a standard tunneling process from the semiconductor valence band.

Qualitatively, the behavior of the threshold bias for the onset of the FN-like photocurrent, V_{th}, as a function of distance can only be understood by including image charge effects. Experimentally, V_{th} is estimated at -2.6, -1.6, and -1.15 V for curves a, b, and c in Fig. 8(b), respectively. Equation (9), which neglects image charge effects, predicts $V_{th} \approx -4.3$ V (using $\phi_m=5.4$ eV for a clean gold surface) which is too large and independent of bias. On the other hand, the experimentally observed thresholds can be understood by using Eq. (15) with tip-sample distances of 1.56, 1.0, and 0.9 nm for curves a, b, and c, respectively.

For curve d of Fig. 8(c), $\ln(I_{ph})$ above 1.5 V is larger than the linear extrapolation from lower bias (dotted line). Despite being in the near-contact regime (see point d of Fig. 5), the excess current is not caused by electrostatic forces acting on
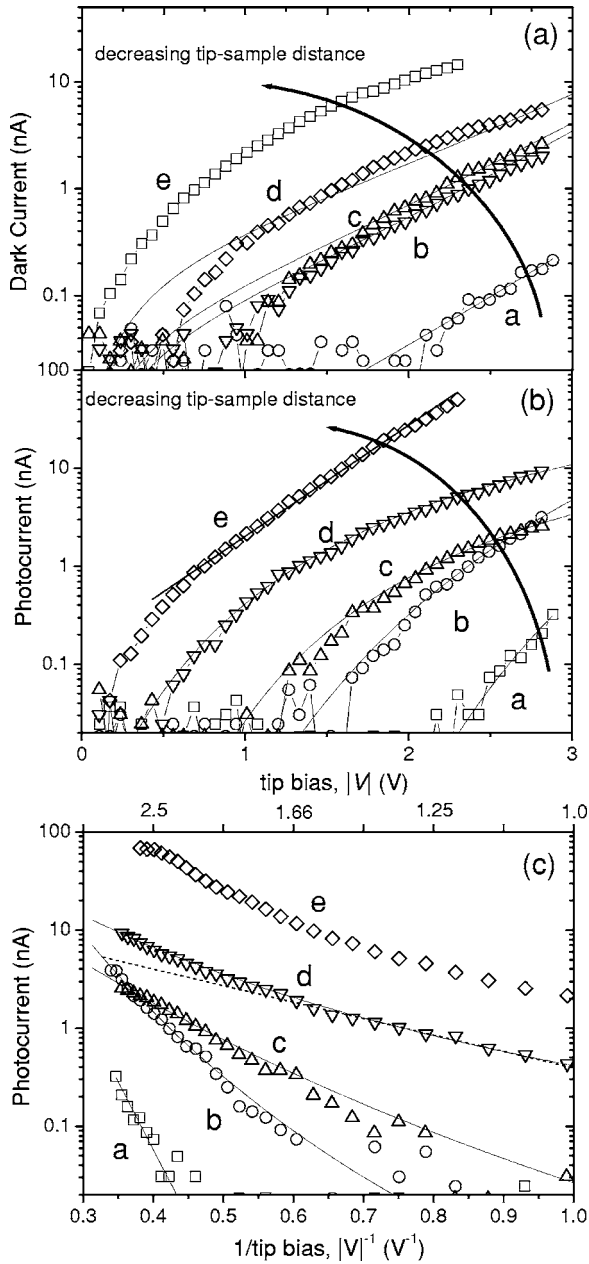
FIG. 8. Plot of the dark current (a) and of the photocurrent (b) as a function of V for the sharp tip shown in Fig. 6. (c) Photocurrent spectra versus $1/V$ show exponential behavior over almost two orders of magnitude. This and the increase in slope with increasing tip-sample distance (from curve d to curve a) indicate a FN-like tunneling process for photoelectrons. The excess photocurrent observed at high tip bias on curve d is also consistent with this interpretation. Solid black curves are fits to the data using Eq. (16) for the dark current and Eq. (13) for the photocurrent (see Sec. V).

the cantilever, as seen from the absence of a bias-dependent atomic force. Rather, it is the result of a lowering of the tunnel barrier due to image charge effects according to Eq. (13).

In the case of curve e of Figs. 8(b) and 8(c), the photocurrent is large. It is estimated that several times 10^{-3} of the total number of photoelectrons created in the tip are injected into the metal. No linear dependence of $\ln(I_{ph})$ as a function

of $1/V$ is observed over the whole bias range. In Fig. 8(b), curve e above a tip bias of 0.5 V shows a simple exponential dependence on tip bias, consistent with the vanishing of the tunnel barrier,[28] and this will be discussed further below. Since the tip is now in mechanical contact with the surface (see Fig. 5), the width of the tunneling gap is constant and equal to the oxide thickness and only the area of the surface indentation, S, changes with set point. When in mechanical contact, it is indeed observed experimentally that $I_{ph}(V)$ and $I_{dark}(V)$ change only by a multiplicative factor with a change in set point.[42]

The dark current bias dependence is found to be approximately exponential at large tip-sample distances [see curves a, b, and c of Fig. 8(a)]. This dependence, which occurs over a small bias range, can be understood by expanding Eq. (17) to first order in V.

V. INTERPRETATION

A. Quantitative analysis of the $I_{ph}(V)$ and $I_{dark}(V)$ bias dependences

A simultaneous fitting procedure, with equal weight, of $I_{ph}(V)$ and of $I_{dark}(V)$ was used, which consisted of selecting initial values of d, ϕ_0, ϕ_m, A_{dark}, and A_{ph}, and in finding the set of values for these quantities that minimizes $R = \Sigma_i [I_{ph}(V_i) - I_{ph}^{calc}(V_i)]^2 + \Sigma_i [I_{dark}(V_i) - I_{dark}^{calc}(V_i)]^2$ where the index i labels the individual data points. The calculated values $I_{ph}^{calc}(V_i)$ and $I_{dark}^{calc}(V_i)$ were obtained using Eqs. (5) and (13) for the photocurrent, and Eq. (16) for the dark current (for which the integral was evaluated numerically). Although there are five fitting parameters, the fit is severely constrained by the fact that both currents depend on d, ϕ_0, and ϕ_m explicitly, as well as indirectly on A_{dark} via the feedback process. This codependence allows for an independent determination of d and ϕ_0 which is not possible in many works on field emission.[17] The fits, shown as solid lines in Fig. 8, are in satisfactory agreement with both the experimental results and the qualitative analysis of the preceding section. The excess photocurrent in curve d at large bias is also accounted for. For the dark current, the small but systematic discrepancy near the threshold may be attributed to the surface barrier V_b at the tip apex. If $|V| < V_b$, the tunneling dark current is reduced because majority carriers must also tunnel across the space charge layer, which is estimated[43] to have a width of order 20 nm.

The values of the parameters obtained using the above procedure, and corresponding to the various curves of Figs. 6(c) and 8 are summarized in Table I.

B. Origin of current instabilities

Examination of the results of Table I concerning curve c of Fig. 6(c) confirms the qualitative analysis of Sec. IV A and suggests the following comments on the nature of the current instabilities.

(i) d takes relatively stable values around 1.2 nm. The magnitude of λ is of the order of 0.4 eV. According to Eq. (15) the lowering of the barrier due to image charge effects cannot be neglected.

TABLE I. Fitting parameters for the curve fits shown in Fig. 8, and for six spectra measured at point c in Fig. 6. A_{ph} influences only the photocurrent, while d, ϕ_0, and ϕ_m are shared between the two according to Eqs. (5), (13), and (16). A_{dark} is an indirectly shared parameter via the feedback loop.

| Spectrum	A_{dark} (A)	A_{ph} (A)	d (nm)	ϕ_0	ϕ_m
a	656	1.9×10^{-6}	1.52	4.4	4.5
b	171	4.1×10^{-6}	1.29	5.1	6.7
c(i)	4.4	6.5×10^{-9}	1.27	4.2	5.3
c(ii)	5.4	7.8×10^{-10}	1.18	3.8	3.3
c(iii)	5.4	5.6×10^{-9}	1.23	4.1	4.7
c(iv)	5.1	3.6×10^{-9}	1.25	4.1	4.9
c(v)	3.9	2×10^{-10}	1.17	3.7	3.2
c(vi)	4.5	4.5×10^{-9}	1.21	4.2	4.9
d	1	1.85×10^{-8}	1.05	4.6	5.7

FIG. 9. Plot of the photocurrent as a function of $1/V$ for the blunt tip shown in Fig. 7. The shared origin indicates that A_{ph} is nearly identical for all four curves taken at different tip-sample distances.

(ii) The values obtained for ϕ_0 and ϕ_m are reasonable: ϕ_0 lies between 3.7 and 4.2 eV and ϕ_m lies between 3.3 and 5.2 eV.

(iii) The largest instability concerns the quantity A_{ph}, which fluctuates by a factor of 30 between the various curves. ϕ_m also fluctuates by about 1.5 eV. In contrast, the fluctuations of A_{dark}, ϕ_0, and d are significantly smaller. Since A_{dark} (and thus S) does not fluctuate, variations in A_{ph} are related to changes in K_{ph}.

The instabilities are presumably related to the fact that the experiments take place in a slightly humid, gaseous environment. With a clean tip and sample surface in vacuum the only possible mechanism for instabilities is the desorption of gold or silicon atoms under the effect of the electric current. This process may explain the observed changes in ϕ_m if desorbed silicon atoms are adsorbed onto the gold surface, but cannot explain the instabilities of K_{ph} which themselves are most reasonably associated with the presence of an oxide layer covering the tip apex. The thickness (d_{ox}) of the oxide is not known, but it is assumed to be smaller than the smallest value found for d in Table I, ≈ 1 nm (the thickness[44] of the planar natural oxide ranges between 0.5 and 1.5 nm).

Since $\epsilon_{SiO_2} = 4$ the electric field is mainly dropped in the tunneling gap between the oxide surface and the metal. The relevant distance for dark current tunneling is still the *total* distance d between the silicon surface of the tip and the metal, whereas for FN-like tunneling, which is an electric-field-driven effect, it is $d - d_{ox}$. In the simplest case where image charge effects are neglected, this results only in a modification of A_{ph}:

$$A_{ph}^* = A_{ph} \exp(\kappa_{ph} d_{ox}), \qquad (19)$$

where κ_{ph} is defined in Eq. (10). Equation (19) provides a possible explanation for the observed variations in A_{ph} as any small variation in d_{ox} translates into large fluctuations in the photocurrent prefactor A_{ph}^*. In the case of the blunt tip, variations in A_{ph} are averaged out over a large surface area: when I_{ph} is plotted against $1/V$ for different tip-sample distances as shown in Fig. 9, the extrapolated curves pass through the
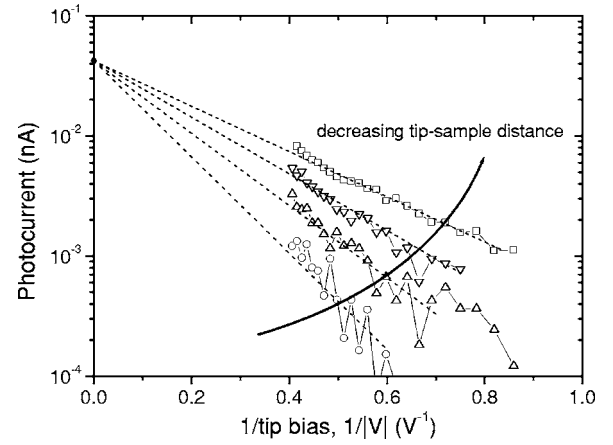
same point at $1/V = 0$ indicating that A_{ph} is nearly identical for all distances. It is partly in consequence of this that fluctuations in the photocurrent [see Fig. 7(b)] are minimal.

The presence of an oxide layer and the inclusion of image charge effects may alter the average $\bar{\phi}$ over the oxide and vacuum barriers and therefore κ_{ph}, but a detailed analysis is unreasonable given the additional adjustable parameters (e.g., oxide thickness, dielectric constant, and effective mass) which are not known if the oxide is ultrathin. The impact of an oxide layer on the results was evaluated using a perturbationlike approach which consisted of introducing an extremely thin oxide (0.1–0.2 nm) into the equations of gradually increasing thickness, and repeating the numerical fit described above. While A_{dark} was increased significantly, the most physically meaningful parameters (d, ϕ_0) were unchanged so the main conclusions of the present work are unaffected if, as assumed above, $d_{ox} \lesssim 0.5$ nm.

Investigations of instabilities in field emission[14] suggest a possible microscopic mechanism for fluctuations in d_{ox}. The tip is thought to be covered by a layer of adsorbed molecules or ions (water, oxygen, etc.) that diffuse into (and out of) the oxide layer under the effect of an electric field, thereby changing its effective thickness. In view of the fact that tunneling occurs via only a handful of atoms or molecules at the tip apex, the observed sharp changes in tunneling current between certain well-defined values can be attributed to the adsorption or desorption of individual molecules. Other explanations involving charge buildup at local defects in the oxide[38,40] can be discounted since this would imply a change in effective barrier height, which, in the majority of cases, is not observed.

C. Effect of tip-sample distance

From Table I d decreases as expected from curve a to curve d. The change in slope of the curves is greater than an $\exp(-d/V)$ dependence and arises from the dependence of λ and thus κ_{ph} on distance.

A_{dark} decreases steadily by almost three orders of magnitude when d is decreased. This might be attributed to a progressive reduction in S with decreasing distance, but a similar trend in A_{ph}, which also depends linearly on S, is not clearly observed perhaps due to the fluctuations in A_{ph}. It may be that A_{dark} is underestimated at small d due to the presence of the oxide layer which is neglected in the model (see the Sec. V B). At small d the relative effect of the oxide is larger and will result in an artificial reduction of A_{dark}. Further studies are necessary to clarify whether this is the case, or whether the trend in A_{dark} is due to a change in K_{dark} (i.e., the orbital overlaps) and/or S.

In the case of curve e of Fig. 8(b), taken under mechanical tip-sample contact, the exponential bias dependence of the tunneling photocurrent can be explained assuming a complete vanishing of the tunnel barrier. Assuming that d is smaller than half the de Broglie wavelength of the electron, and taking a square barrier, it has been recognized (see Fig. 2.6 of Ref. 28) that the probability of ballistic transmission is an exponential function of the barrier height. Taking the barrier height to be the spatial average calculated using Eq. (4), the probability for ballistic transmission is of the form

$$T = \exp\{-(\bar{\phi} - E_g)/\phi^*\}, \tag{20}$$

where ϕ^* is some characteristic energy. Again using Simmons' approximation for the image charge potential Eq. (11), the ballistic photocurrent is of the form

$$I_{ph} = A_{ph} \exp\{-(\chi_0/2 + 2.8\lambda - aqV^*/2)/\phi^*\}. \tag{21}$$

The barrier given by Eq. (11) only vanishes if λ is larger than about 0.5 eV (this assumes for simplicity that $\phi_0 = \phi_m = 4$ eV). Taking an oxide thickness of 0.5 nm as suggested by Sec. V B, and $\epsilon_{SiO_2} = 4$, Eq. (12) yields $\lambda = 0.25$ eV which is too small. However, the dielectric constant of the ultrathin oxide layer may be smaller than the bulk value, so $\lambda \approx 0.5$ eV is reasonable. Using this value and taking the oxide effective mass as given in Ref. 45, a de Broglie wavelength for $V = -2$ V of the order of 3 nm is obtained, which is indeed larger than twice d_{ox}. Similarly, using Fig. 2.6 of Ref. 28, ϕ^* is calculated to be 0.025 eV. In view of uncertainties in the value of d_{ox} and in the shape of the barrier, the agreement with the experimental value of 0.1 eV can be considered as satisfactory.

D. Comparison with other works

In the model of Ref. 12, all tunneling occurs via midgap surface states uniformly distributed in energy and is formulated for low tip bias. This mechanism, illustrated in Fig. 2 (arrow 3), can be excluded here for two reasons. (i) The most significant tip bias dependence of the tunneling current in the model of Ref. 12 arises via the bias dependence of the surface depletion layer width,[24] and is too weak to explain the strong variation observed in this work. Extension of the model of Ref. 12 to include the bias dependence of κ_{ph}, given by Eq. (7), is also unable to explain the results. (ii) The tunneling photocurrent in the model of Ref. 12 depends logarithmically on the incident light power in contrast with the linear dependence observed here (see Fig. 10).
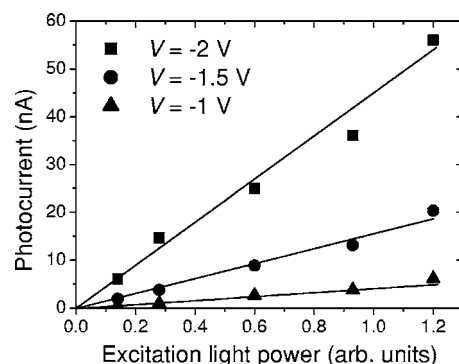

FIG. 10. Dependence of the photocurrent on excitation light power. For the three values of the tip bias, this dependence is linear.

Besides the tip bias values used in Ref. 12, which are too small to observe FN-like tunneling, their use of GaAs tips is also significant. In defect-free GaAs the surface recombination velocity is orders of magnitude larger than that for defect-free silicon.[46] Consequently, the characteristic time for trapping at midgap states may be faster than the characteristic tunneling time from the conduction band so tunneling will proceed via midgap states. The opposite may be true in silicon so that FN-like tunneling is favored.

VI. CONCLUSION

Photoassisted tunneling between a *p*-type silicon tip illuminated from the rear and a metallic gold surface has been studied for absolute tip bias up to 3 V. The additional tunneling current induced by light excitation, due to injection of photocarriers from the tip into the surface, is large and comparable with the dark current. Its magnitude depends linearly on the light excitation power and no surface photovoltage is observed.

The tunneling dark and photocurrent spectra are distinct and are quantitatively interpreted by a simple model that yields reasonable values of the tip and metal work functions and of the tip-sample distance. The tunneling dark current is described by a standard process between the semiconductor valence band and the metallic density of states. In contrast, the tunneling photocurrent behavior is explained by an electric-field-dependent FN-like process between the semiconductor conduction band and the metallic density of states, including image charge effects. This mechanism accounts for all the results obtained before mechanical tip-sample contact: the $\exp(1/V)$ dependence of the tunnel photocurrent at large tip-sample distance, as well as the excess current at large tip bias observed just before contact. Once in contact the tunnel barrier for photoelectrons vanishes, and current flow is determined by the probability of ballistic emission over the barrier. This results in a photocurrent dependent exponentially on V.

For spin injection applications with GaAs tips,[5–7] it is possible that at low bias injection will be best described by the standard-tunneling-based model of Ref. 12 However, the present work indicates that FN-like tunneling may also be observed at higher tip bias, even with GaAs. FN-like tunnel-

ing is likely to be spin dependent since the vacuum states into which photoelectrons tunnel should be hybridized with the spin-polarized states of the magnetic surface. In this case, FN-like tunneling would then be the relevant process (for example) for studies of the highly polarized minority-spin d states of Fe and Co surfaces which lie about 2 eV above the Fermi level.[47]

In common with many works on field emission from silicon tips and on transport through Si/SiO_2 structures, current instabilities are observed. However, since the instabilities tend to occur over time scales longer than that taken for the spectral measurements of both the tunneling dark current and the tunneling photocurrent, a meaningful analysis of the spectra is possible. With the aid of the model developed here, it is possible to show that the current instabilities are mostly related to changes in the thickness of the oxide layer covering the tip apex. Changes in this thickness may be related to electric-field-induced adsorption or desorption of foreign species such as water or oxygen. For this reason, an appropriate surface passivation of the tip is essential for future spin-polarized injection investigations using GaAs tips in liquid or neutral gas environments. Studies are under way to optimize such a tip treatement.[48]

APPENDIX: NEGLIGIBLE FIELD ENHANCEMENT AT THE TIP APEX

When discussing field emission phenomena, it is usual to describe the effect of tip geometry on the electric field by introducing the enhancement factor γ defined by $F_{apex} = \gamma V/d$, where F_{apex} is the electric field at the tip apex. There is currently great interest in the use of sharp tips and high-aspect-ratio objects such as carbon nanotubes, where field enhancement factors up to $\gamma=10^4$ are reported,[17] since these
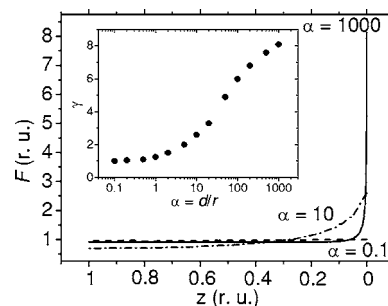

FIG. 11. Variation in normalized electric field (units of V/d) along the axis from the tip ($z=0$) to the sample surface ($z=1$ reduced unit). A large increase in electric field is observed close to the tip for large α. The inset shows the variation in γ with the aspect ratio $\alpha=d/r$. For small values of α, corresponding to the experiments reported here, $\gamma \rightarrow 1$.

make for very efficient field emitters. In the present case γ is of order unity despite the fact that sharp tips are used. The main difference here is that the tip-sample distance d is of order 1 nm (i.e., smaller than the tip radius $r \approx 60$ nm), whereas in field emission studies the cathode-anode distance can be as large as several micrometers (i.e., much larger than the tip radius). At the scale of 1 nm therefore, the "sharp" tips used in this study are locally flat and $\gamma \approx 1$.

The electric field $F(z)$ has been calculated along the axis between the tip apex and the surface. This calculation was performed numerically in two dimensions, using a finite-element resolution of Laplace's equation, with a fixed potential difference V between tip and sample. The tip is modeled as a conical section of half angle 12°, similar to the value for the tips used in the experiments, and the tip apex is terminated by a circle of radius r. As shown in Fig. 11, for $\alpha = 10^3$, which corresponds to a typical field emission experiment, the electric field is greatly enhanced near the tip surface where $\gamma \approx 8$. For $\alpha=10^{-1}$ which corresponds to the present tunneling experiments, $F(z)$ is constant and $\gamma=1$. The variation in γ with α is shown in Fig. 11 (inset). It is noted that γ deviates from unity only for α larger than 1.

*Electronic address: daniel.paget@polytechnique.fr

[1] S. Grafström, J. Appl. Phys. **91**, 1717 (2002).

[2] O. J. Glembocki, E. S. Snow, C. R. K. Marrian, S. M. Prokes, and D. S. Katzer, Ultramicroscopy **42**, 764 (1992).

[3] R. J. Hamers and K. Markert, Phys. Rev. Lett. **64**, 1051 (1990).

[4] G. Lampel, Phys. Rev. Lett. **20**, 491 (1968).

[5] D. T. Pierce, Phys. Scr. **38**, 291 (1988).

[6] D. P. DiVincenzo and D. Loss, J. Magn. Magn. Mater. **200**, 202 (1999).

[7] S. Datta and B. Das, Appl. Phys. Lett. **56**, 665 (1990).

[8] S. F. Alvarado, Phys. Rev. Lett. **75**, 000513 (1995).

[9] R. Jansen, R. Schad, and H. van Kempen, J. Magn. Magn. Mater. **199**, 668 (1999).

[10] W. Nabhan, Y. Suzuki, R. Shinohara, K. Yamaguchi, and E. Tamura, Appl. Surf. Sci. **145**, 570 (1999).

[11] M. Bode, Rep. Prog. Phys. **66**, 523 (2003).

[12] M. W. J. Prins, R. Jansen, R. H. M. Groeneveld, A. P. van Gelder, and H. van Kempen, Phys. Rev. B **53**, 8090 (1996).

[13] R. Jansen, M. W. J. Prins, and H. van Kempen, Phys. Rev. B **57**, 4033 (1998).

[14] N. Miyamoto, H. Adachi, H. Nakane, and K. Yamane, J. Vac. Sci. Technol. B **21**, 436 (2003).

[15] B. Günther, F. Kaldasch, G. Müller, S. Schmitt, R. Henning, R. Huber, and M. Lacher, J. Vac. Sci. Technol. B **21**, 427 (2003).

[16] R. G. Forbes, J. Vac. Sci. Technol. B **17**, 534 (1999).

[17] J.-M. Bonard, K. A. Dean, B. F. Coll, and C. Klinke, Phys. Rev. Lett. **89**, 197602 (2002).

[18] K. L. Jensen, Y. Y. Lau, and D. McGregor, Appl. Phys. Lett. **77**,

585 (2000).

[19] R. H. Fowler and L. W. Nordheim, Proc. R. Soc. London, Ser. A **119**, 173 (1928).

[20] A. Filipe, H.-J. Drouhin, G. Lampel, Y. Lassailly, J. Nagle, J. Peretti, V. I. Safarov, and A. Schuhl, Phys. Rev. Lett. **80**, 2425 (1998).

[21] H. A. Schwettman, J. P. Turneaur, and R. F. Waites, J. Appl. Phys. **45**, 914 (1974).

[22] R. S. Becker, J. A. Golovchenko, and B. S. Swartzentruber, Phys. Rev. Lett. **55**, 987 (1985).

[23] Y. Suzuki, W. Nabhan, R. Shinohara, K. Yamaguchi, and T. Katayama, J. Magn. Magn. Mater. **198**, 540 (1999).

[24] W. W. Gärtner, Phys. Rev. **116**, 84 (1959).

[25] The geometry in which the tip is excited from the planar rear surface of the tip is favorable for the elimination of the parasitic optical effects that have plagued all efforts aimed at observing spin-dependent tunnel processes between a semiconducting tip and a magnetic surface.

[26] D. Paget, J. Peretti, A. C. H. Rowe, G. Lampel, B. Gérard, and S. Bansropun, European Patent No. 05 05394 (2005).

[27] J. G. Simmons, J. Appl. Phys. **34**, 1793 (1963).

[28] C. Julian Chen, *Introduction to Scanning Tunneling Microscopy* (Oxford University Press, New York, 1993).

[29] This approximation is straightforward for photoelectrons for which the kinetic part of the energy is very small, so that $E \approx E_z$. For the dark tunneling current, the corrected form of Eq. (16) is obtained by replacing E_z by $E\cos^2 \theta$ and d by $d/\cos \theta$ where θ is the angle between the tip axis and the electron momentum k. For realistic values of d and ϕ_0, the tunneling current rapidly decreases with θ, with a half width at half maximum $\theta_m \approx 15°$. Since θ_m is weakly dependent on both E and V^*, and since $\cos \theta_m$ is close to unity, the only effect of the angular dependence of the tunneling probability is to add a bias-independent prefactor, proportional to θ_m.

[30] As seen from Eq. (4), the value of $\bar{\phi}$ depends on the spatial limits d_1 and d_2 of the barrier. Simmons (Ref. 27) takes d_1 and d_2 at the Fermi level. Here, expressions for d_1 and d_2 are calculated at the energy E_g of the tunneling photoelectrons, and are found by replacing ϕ_0 by $\phi_0 - E_g$ in Eq. (36) of Ref. 27.

[31] The tip bias should be large enough that d_2 can be determined by Eq. (38) of Ref. 27, otherwise Eq. (37) of the same work should be applied. The condition $qV > \phi_0$, cited by Simmons for the crossover between the two regimes, corresponding to the threshold bias for FN-like tunneling, is erroneous. By equating the expressions given in Eqs. (37) and (38), and replacing ϕ_0 by the smaller χ_0, it is found that Eq. (38) of Ref. 27 is valid even at tip bias as low as 1 V, especially when image charge effects (i.e., λ) are large. A rather inelegant expression for V_{th} is obtained.

[32] Using Eq. (37) of Ref. 27, the modification of the spatial average of the tunneling barrier due to image charge effects is found to be negligible.

[33] D. A. Papaconstantopoulos, *Handbook of the Band Structure of Elemental Solids* (Plenum Press, New York, 1986).

[34] Since at this energy the light absorption length is comparable with the tip height, some electrons are created in the subapex region. However, because of the high tip doping level, only a small fraction of the photocurrent originates from electrons photocreated in the depletion zone and the photocurrent can still be assumed to be independent of bias.

[35] Dlevers from Veeco (https://www.veecoprobes.com). In order to improve the coupling of the pump light to the tip, the metallic layer on the rear face of the cantilever was removed.

[36] P. Prod'homme, F. Maroun, R. Cortès, P. Allongue, J. Hamrle, J. Ferré, J. Jamet, and N. Vernier (unpublished).

[37] N. A. Burnham and R. J. Colton, J. Vac. Sci. Technol. A **7**, 2906 (1989).

[38] K. R. Farmer, C. T. Rogers, and R. A. Buhrman, Phys. Rev. Lett. **58**, 2255 (1987).

[39] K. R. Farmer, R. Saletti, and R. A. Buhrman, Appl. Phys. Lett. **52**, 1749 (1988).

[40] C. T. Rogers and R. A. Buhrman, Phys. Rev. Lett. **55**, 859 (1985).

[41] The overall amplitude of $I_{dark}(V)$ is imposed by the feedback loop, and cannot be considered as an adjustable parameter.

[42] Since the $I_{ph}(V)$ and $I_{dark}(V)$ spectra change only by a multiplicative factor, the potential drop in the tip and cantilever is still negligible with respect to the applied tip bias.

[43] The depletion layer width at the tip apex is estimated numerically at almost a factor of 10 larger than that calculated for a planar contact.

[44] G. Xiaoge Zhang, *Electrochemistry of Silicon and Its Oxide* (Plenum, New York, 2001).

[45] B. Brar, G. D. Wilk, and A. C. Seabaugh, Appl. Phys. Lett. **69**, 2728 (1996).

[46] R. A. Smith, *Semiconductors* (Cambridge University Press, Cambridge, England, 1978).

[47] J. A. Stroscio, D. T. Pierce, A. Davies, R. J. Celotta, and M. Weinert, Phys. Rev. Lett. **75**, 2960 (1995).

[48] V. L. Berkovits, D. Paget, A. N. Karpenko, V. P. Ulin, and O. E. Tereshchenko, Appl. Phys. Lett. **90**, 022104 (2007).